ISSN 2517-7516, Membranes and Membrane Technologies, 2022, Vol. 4, No. 1, pp. 23–30. © Pleiades Publishing, Ltd., 2022.
Russian Text © The Author(s), 2022, published in Membrany i Membrannye Tekhnologii, 2022, Vol. 12, No. 1, pp. 29–37.

A Study of the Degradation of a Perfluorinated Membrane during Operation in a Proton-Exchange Membrane Fuel Cell

D. S. Kudashova[a], N. A. Kononenko[a], M. A. Brovkina[a], and I. V. Falina[a, *]

[a] *Kuban State University, Krasnodar, 350040 Russia*

**e-mail: irina_falina@mail.ru*

Received September 7, 2021; revised October 1, 2021; accepted October 8, 2021

Abstract—Results of a study of the transport and structural characteristics of an MF-4SK membrane at different stages of membrane operation as part of the membrane electrode assembly of a proton-exchange membrane fuel cell have been described. Membrane degradation has been assessed by the membrane conductometry and voltammetry, standard contact porosimetry, and optical microscopy methods. A quantitative assessment of the effect of a thermomechanical impact exerted during the pressing of the membrane electrode assembly and the different conditions of the assembly operation on the thickness, exchange capacity, water uptake, pore structure characteristics, electrical conductivity, and current–voltage curve parameters of the membrane has been conducted. The main factors that have the most significant effect on the degradation of the perfluorinated membrane have been identified.

Keywords: perfluorinated membrane, electrical conductivity, exchange capacity, porosimetric curve, current–voltage characteristic, membrane electrode assembly, proton-exchange membrane fuel cell

DOI: 10.1134/S251775162201005X

INTRODUCTION

The most promising alternative sources of electrical energy include low-temperature proton-exchange membrane fuel cells [1]. Their undoubted advantage is high efficiency and the absence of harmful and hazardous emissions into the atmosphere. However, their widespread implementation is complicated by both the cost of the generated electrical power and the lack of stable and highly efficient materials [2, 3]. One of the key components of a proton-exchange membrane fuel cell is a proton-exchange membrane; the materials that are conventionally used as these membranes are perfluorinated sulfonated cation-exchange polymers, such as Nafion (DuPont, United States) or the MF-4SK membrane (Russian counterpart). The present-day studies in the field of low-temperature fuel cells are aimed at improving all components of the membrane electrode assembly (MEA), namely, the proton-exchange membrane and the catalyst bed that is in direct contact with the membrane.

The main causes of a decrease in the characteristics of proton-exchange membrane fuel cells are changes in the properties of the catalyst [1, 4–7], primarily, at the cathode [2]. The catalyst degradation is attributed to a decrease in the catalyst activity due to a decrease in the catalyst surface owing to the coarsening of the nanoparticles, the irreversible oxidation of a portion of the active sites, and the degradation of the carbon support [4, 5, 8]. Studying of the mechanisms of these processes is a scientific direction of current concern.

In addition to the adverse processes that occur in the catalyst, a deterioration of the properties of the polymer electrolyte can occur [7, 9–13]; this factor should also be taken into account in developing a fuel cell. The degradation processes that occur in the membrane can be divided into two groups: the degradation of the polymer and the appearance of impurities that worsen the transport characteristics of the membrane. Currently, several causes of membrane degradation are discussed in the literature. On the one hand, the proton-exchange membrane can be contaminated with extraneous cations, which penetrate into the MEA with an air or fuel stream [14, 15] or are formed due to the partial oxidation of the structural elements of the MEA [16–18]. Another source of extraneous cations is catalysts based on alloys of platinum with *d*-elements; in recent years, doping with these elements has been commonly used to increase the specific activity of the catalysts in current-generating reactions and decrease the cost of electrocatalysts [19–21]. The authors of [18] report that membranes can be contaminated with nanoparticles of some elements, such as Pt, Ir, Ti, Fe, and Ni, whose cations are formed during the oxidation of the MEA components, migrate into the membrane, and are reduced by hydrogen that penetrates into the membrane via the crossover mechanism. Thus, during the corrosion of

platinum as part of the cathode catalyst, Pt^{2+} and Pt^{4+} cations can migrate into the membrane and undergo hydrogen reduction to form a platinum strip in the membrane from the cathode side [6, 9]. Another cause is the degradation of the polymer chains by peroxo compounds formed in the oxygen electroreduction reaction [9, 22–24], which leads to a decrease in the thickness [25] and exchange capacity of the membrane [2]. However, the contribution of each of the degradation mechanisms of the MEA and, in particular, the proton-exchange membrane, has not yet been fully identified. The aim of this study was to explore the degradation of an MF-4SK proton-exchange membrane by studying a number of the physicochemical characteristics of the membrane at different stages of operation of the MEA of a proton-exchange membrane fuel cell. The task included a comprehensive study of the electric transport and structural properties of the proton-exchange membrane by the membrane conductometry and voltammetry, standard contact porosimetry (SCP), and optical microscopy methods.

EXPERIMENTAL

Object of Research

The object of the study was an MF-4SK perfluorinated membrane (OOO Plastpolymer, St. Petersburg), which was used as a polymer electrolyte for the MEA. The following samples were studied: an original membrane (MF-4SK), a membrane after pressing during the construction of the MEA (MF-4SK-P sample), and membranes after life tests in two modes: potentiostatic for 100 h (hereinafter, mode 1, sample MF- 4SK-R1) and potentiodynamic (mode 2, sample MF-4SK-R2). The transport and structural characteristics of the membranes were studied at each stage of the construction and operation of the MEA: immediately after pressing and after life tests in modes 1 and 2. Before the construction of the MEA, the membranes were boiled in distilled water for 3 h, immersed into a 1 M sulfuric acid solution to convert into the proton form, and washed with distilled water, while controlling the water resistance over the membrane.

Construction and Testing of the MEA of a Fuel Cell

In all the cases, the catalytic ink was prepared using a commercial E-TEK-C1-40 catalyst (40% Pt on the Vulcan XC-72 carbon black). The catalytic mixture for depositing on the electrodes consisted of a weighed portion of the catalyst, a 10% dispersion of Nafion in isopropanol (Nafion content was 12.5% of the weight of the catalyst), distilled water, and isopropanol in a ratio of 8 : 1. The resulting mixture was dispersed in an ultrasonic bath for 60 min. After that, a 280-μm-thick Toray EC-TP1-090T carbon paper was placed on a predegreased plate, the surface of which was heated to 60°C, and the catalytic ink was uniformly deposited on one of the surfaces of the paper. The area of each electrode was 5 cm^2. Membrane electrode assemblies were prepared by hot pressing of gas-diffusion layers with a catalyst bed predeposited on them and an air-dried MF-4SK proton-exchange membrane at a temperature of 117–120°C. The pressing was conducted at a pressure of 80 atm for 3 min. The loading of the two electrodes with platinum was 0.3 mg/cm^2.

The life tests of the MEA were conducted at 25°C without further humidifying the gases in two modes: (mode 1) at a load voltage of 0.5 V for 100 h and (mode 2) 10000 cycles of accelerated stress testing with triangular pulses in a voltage range of 0.6–1.2 V at a potential sweep rate of 0.1 V/s. Mode 1 implied mild testing conditions providing the partial regeneration of the membrane after the pressing stage. Mode 2 implied stress testing under severe conditions providing the exposure of all MEA components to significant adverse impacts. The application of 2500 cycles in the selected stress testing mode is equivalent to the conduction of life tests for 1010 h [2]. Electrochemical impedance spectra were measured in a frequency range of 0.1 Hz to 500 kHz before testing and every 2000 cycles. The impedance spectra were used to determine the ohmic resistance of the MEA. In studying all the electrochemical characteristics of the MEA, the flow rate of hydrogen and air into the cell was maintained constant at a level of 20 and 180 L/h, respectively. The electrochemical characteristics of the MEA were studied using a P-45X potentiostat-galvanostat equipped with a FRA-24M frequency response analyzer module (Electrochemical Instruments, Chernogolovka, Russia).

After the life tests, the MEA was disassembled, the membrane was placed in distilled water, the catalyst was removed from the membrane surface, and then the properties of the polymer electrolyte were studied.

Physicochemical Characteristics of the Membrane

The exchange capacity of the membrane samples (Q, mmol/g) was determined in accordance with a standard procedure by the equilibrium displacement method with excess titrant. The experimentally determined Q value was recalculated per gram of dry membrane. Membrane thickness (l, mm) was measured with an MK-25 0.01 micrometer.

The conducting properties of the perfluorinated membranes were determined by the mercury contact probing method described in [26]. To measure the concentration dependences of electrical conductivity, the samples were pretreated: they were brought into equilibrium with sulfuric acid solutions of different concentrations. Membrane resistance was determined from the active part of the impedance in a frequency range of 0.1 Hz to 500 kHz. The error in determining the resistance of the samples did not exceed 5%.

The current–voltage characteristics of the membranes were measured in a four-chamber flow-

through electrodialysis cell. During the experiment, the test membrane was separated from the electrode chambers with an auxiliary cation-exchange (MK-40) and anion-exchange membrane (MA-41). A sulfuric acid solution with a concentration of 0.05 mol-equiv/L was pumped through all chambers of the electrodialysis cell at a rate of 10 mL/min. The intermembrane distance was 0.73 cm; the polarizable membrane area was 2.38 cm^2. A direct current was applied to the platinum polarizing electrodes. Membrane potential was measured using Luggin capillaries that were connected to silver chloride electrodes connected to the geometric centers of the polarized regions of the test membrane and located at a distance of about 0.8 mm from the membrane surface. Current–voltage characteristics were determined from chronopotentiograms as dependences of the time-average steady-state potential jump on the current density. The procedure for recording current–voltage characteristics and chronopotentiograms is described in detail in [27].

The binding energy and effective pore radius distribution of water in the membranes was studied by the SCP method [28, 29]. Using this method, it is possible to study the pore structure of materials in a pore radius range of 1 nm to 300 μm, which is wider than the range that can be studied using other structure-sensitive methods. The method consists in measuring the equilibrium curve of relative water uptake for a sample contacting with a reference sample, for which the porosimetric curve was prerecorded by an independent method. The experimental procedure is described in detail in [30, 31].

A number of pore structure characteristics were determined from the recorded porosimetric curves in the integral and differential form. The maximum water uptake value (V_0, cm^3/g) characterizes the total pore volume in the membrane. Using the determined V_0 value and the exchange capacity of the membrane, the specific water uptake was calculated as the number of water moles per mole of sulfo groups of the membrane (n, $mol_{H_2O}/mol^-_{SO_3}$):

$$n = \frac{V_0}{Q\,V_m}, \tag{1}$$

where V_m is the molar volume of water of 18 cm^3/mol.

The internal specific surface area of macro- and mesopores with an effective radius of more than 1 nm (S_1) was calculated by the following formula [31]:

$$S_1 = 2\int_{r=1}^{r_{max}} \frac{1}{r^2}\left(\frac{dV}{d\ln r}\right)dr = 2\int_{r=1}^{r_{max}} \frac{dV}{r}. \tag{2}$$

The contribution of micropores with $r \le 1$ nm to the internal specific surface area (S_2) was approximately assessed by the following formula [31]:

$$S_2 = \frac{2V_{min}}{r_{min}}, \tag{3}$$

where $r_{min} = 1$ nm and V_{min} is the respective pore volume.

The total internal specific surface area (S) was determined as the sum of the above two terms: $S = S_1 + S_2$.

The data on the exchange capacity of the membrane were used to calculate the average distance between the fixed groups (L) and the charge density at the internal interface (q):

$$L = \sqrt{\frac{S}{QN_A}}, \tag{4}$$

$$q = \frac{QF}{S}, \tag{5}$$

where N_A is the Avogadro's number.

Images of surfaces of the membranes in a swollen state were recorded using an Altami BIO 2 optical microscope with a 10× magnification; the microscope was equipped with a digital ocular USB camera.

RESULTS AND DISCUSSION

Characteristics of the MEA

Results of the life tests of the MEA under mild testing conditions (mode 1), which make it possible to partly regenerate the membrane after the pressing stage, and under more severe conditions (mode 2), which are equivalent to long-term life tests, are shown in Figs. 1a and 1b, respectively. For mode 2, the current density is shown at an applied potential difference of 0.6 V. It is evident from Fig. 1a that, during the operation of the MEA in test mode 1, the current density increases to a value of 70 mA/cm^2. At the same time, during the operation of the MEA in mode 2, the current density significantly decreases even after 1000 cycles and remains almost constant during further operation.

Results of measuring the resistance of the MEA during testing under the different conditions taking into account the real time of the test in the stress testing mode are shown in Fig. 2. It is evident from the figure that the resistance of the MEA operating in the potentiodynamic mode is significantly higher than that in the potentiostatic mode.

Physicochemical and Structural Characteristics of the Polymer Electrolyte

The physicochemical characteristics of the membrane were determined at each stage of the construction and operation of the MEA. Table 1 lists the thicknesses of four samples of the original MF-4SK membrane in a swollen state (l_0). Despite the fact that the samples were cut from one sheet, their thickness varies in a range of 0.20–0.23 mm. The thickness of the membrane in a swollen state after use in the MEA (l_1) is also shown in Table 1. It is evident from the table

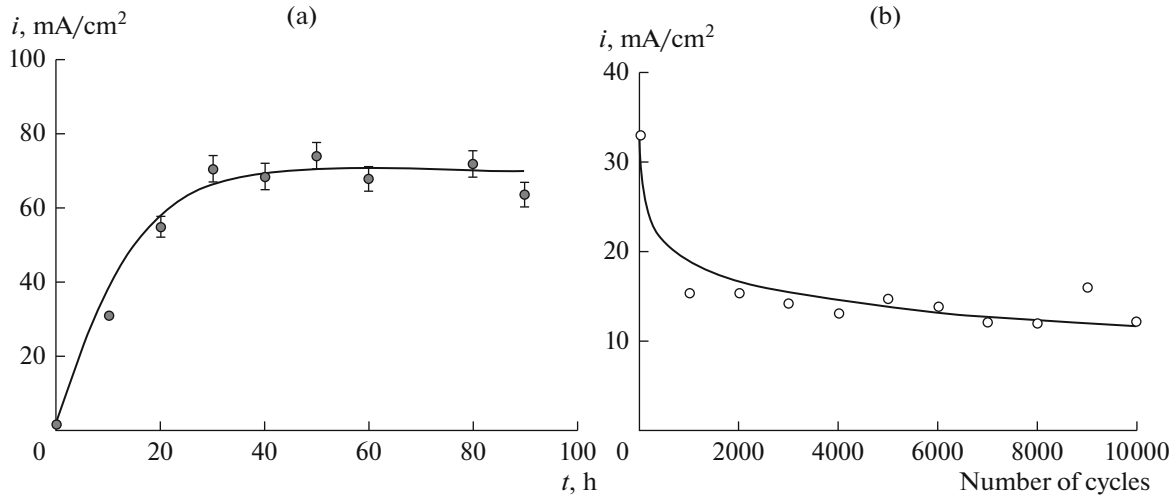

Fig. 1. Variation in the current density during testing the MEA in modes (a) 1 and (b) 2.

that thermal and mechanical impacts on the membrane during pressing in the MEA construction process leads to a decrease in the membrane thickness by about 10%. During the further operation of the membrane as part of the MEA, the membrane thickness remains almost unchanged. At the same time, the MEA pressing stage has no effect on the exchange capacity of the membrane (Table 1). An 8% decrease in the exchange capacity was observed for the MF-4SK-R2 membrane after operation under severe stress testing conditions. This decrease can be attributed to the elimination of some of the functional SO_3 groups by peroxo compounds formed in the oxygen electroreduction reaction.

For all the studied membrane samples, Fig. 3 shows curves of the effective pore radius distribution of water; the structural characteristics calculated from the curves are shown in Table 1. It is evident from the results that the most significant changes in the structure of the MF-4SK membrane occur during pressing in the MEA construction process. The thermal and mechanical impacts exerted on the membrane during pressing lead to a 28% decrease in the total pore volume. As a consequence, the specific water uptake of the membrane also decreases by 28%. The resulting decrease in the internal specific surface area is accompanied by a regular decrease in the distance between the functional groups and an increase in the charge density at the internal phase interface. During the operation of the membrane in a fuel cell, the structural characteristics of the membrane hardly change any longer.

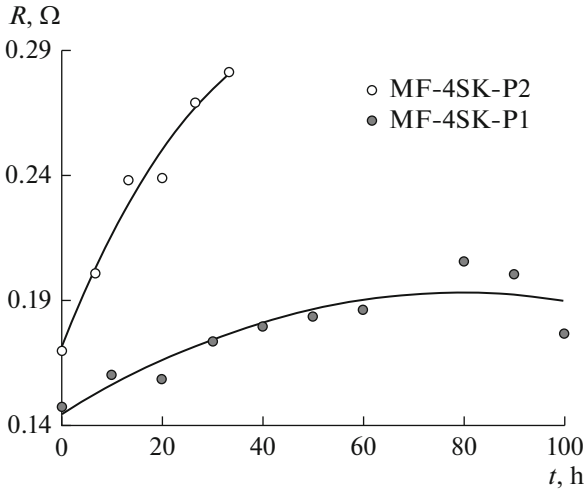

Fig. 2. Dependence of the membrane resistance on the test time in modes 1 and 2.

Figure 4 shows the concentration dependences of the electrical conductivity of the membranes in a sulfuric acid solution. Analysis of the recorded dependences showed that the electrical conductivity of all the samples decreases about twofold in the entire concentration range compared to the electrical conductivity of the original membrane; this fact is associated with a decrease in both the maximum and specific water uptake of the membranes.

Using the concentration dependences of the electrical conductivity, the transport and structural parameters of a microheterogeneous model of an ion-exchange membrane were calculated. According to this model [26], the structure of an ion-exchange membrane is regarded as a two-phase conducting system containing a gel phase and an intergel solution phase. In the gel phase, which is assumed to include all components of an ion-exchange membrane, except for the equilibrium solution, the current is transferred only by counterions. In the intergel spaces filled with an electrically neutral solution, the current is transferred by both cations and anions. The electrical con-

Table 1. Physicochemical and structural characteristics of the MF-4SK membrane at the different stages of operation in a fuel cell

No.	Membrane	l_0, mm	l_1, mm	Q, mmol/g_{dry}	V_0, cm^3/g	n, mol H_2O/mol SO_3^-	S, m^2/g	L, nm	q, C/m^2
1	MF-4SK	0.235 ± 0.003	0.235 ± 0.003	0.87	0.36	23.0	236	0.65	0.38
2	MF-4SK-P	0.204 ± 0.007	0.183 ± 0.006	0.86	0.26	16.8	195	0.61	0.43
3	MF-4SK-R1	0.211 ± 0.007	0.202 ± 0.004	0.87	0.24	15.3	198	0.61	0.42
4	MF-4SK-R2	0.207 ± 0.006	0.182 ± 0.004	0.80	0.24	16.7	188	0.63	0.41

ductivity of this system is described by the following equation [32]:

$$\kappa_m = \kappa_{iso}^{f_1} \kappa_{sol}^{1-f_1}, \quad (6)$$

where f_1 is the volume fraction of the gel containing polymer chains, hydrated fixed ions, and counterions; f_2 is the volume fraction of the free solution, $f_1 + f_2 = 1$; and κ_{iso} and κ_{sol} are the conductivity of the gel phase and intergel solution, respectively. The processing of the concentration dependences in the $\log\kappa_m = f(\log\kappa_{sol})$ coordinates makes it possible to determine the values of these parameters. The calculated values of the transport and structural parameters are listed in Table 2.

It is evident from Table 2 that the electrical conductivity of the gel phase of the membrane decreases about twofold even after pressing. This decrease in κ_{iso} is attributed to a decrease in the water uptake of the samples, in particular, the hydration capacity of the gel phase, and, as a consequence, a decrease in the mobility of counterions in the gel. The most significant decrease in the conductivity of the gel is observed for the MF-4SK-R2 sample; this finding can be attributed to the fact that the exchange capacity of this sample is lower than that of the other samples. However, the volume fractions of the conducting phases change proportionally, and the ratio between them remains constant. This fact suggests that the membrane is uniformly compressed during pressing. Earlier, the authors of [33], in studying a wide range of membranes of various structural types, observed a similar effect of the invariability of the f_1 and f_2 parameter values with an increase in the solution concentration despite a decrease in the water uptake of the membranes.

Figure 5 shows the current–voltage characteristics of the membranes in a 0.05 mol-equiv/L sulfuric acid solution. It is evident from the figure that the curves have a classical shape and contain the following three regions: an ohmic region, a limiting current plateau,

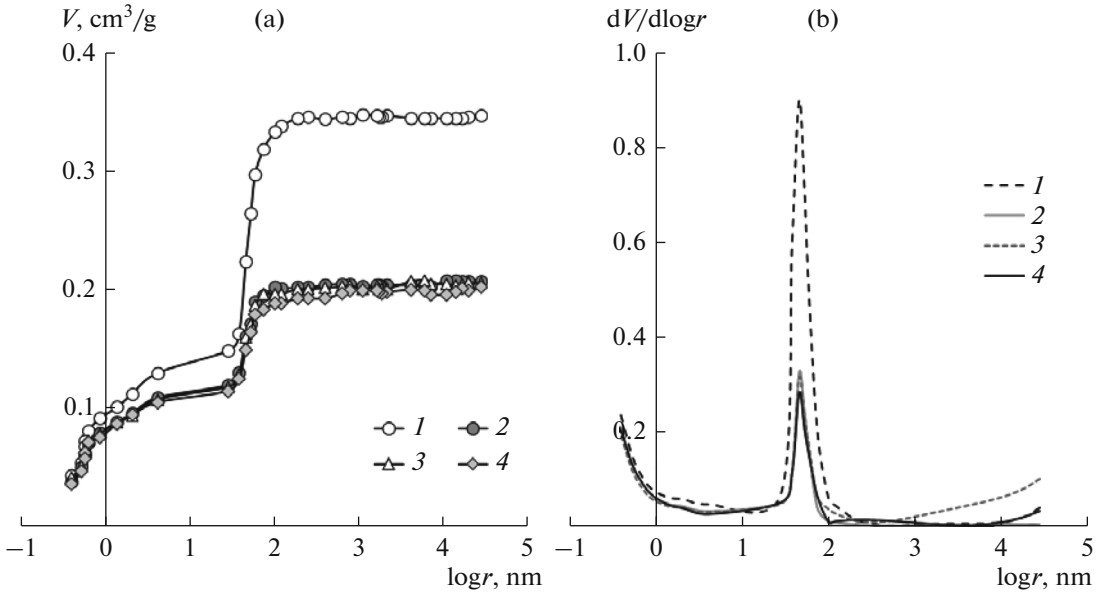

Fig. 3. (a) Integral and (b) differential curves of the pore radius distribution of water: (*1*) MF-4SK, (*2*) MF-4SK-P, (*3*) MF-4SK-R1, and (*4*) MF-4SK-R2.

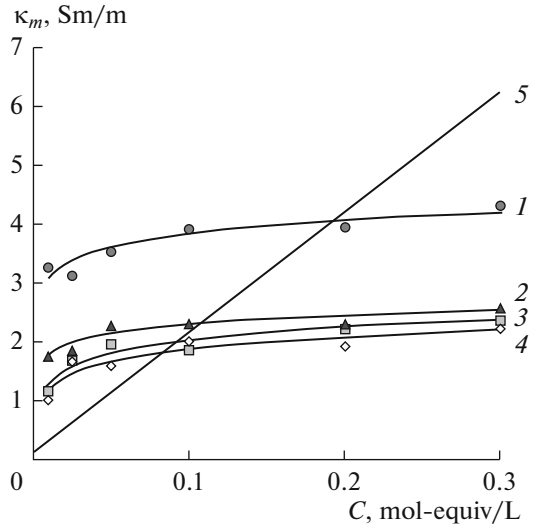

Fig. 4. Concentration dependences of the electrical conductivity of membrane samples in a sulfuric acid solution: (*1*) MF-4SK, (*2*) MF-4SK-R1, (*3*) MF-4SK-P, (*4*) MF-4SK-R2, and (*5*) an H_2SO_4 solution.

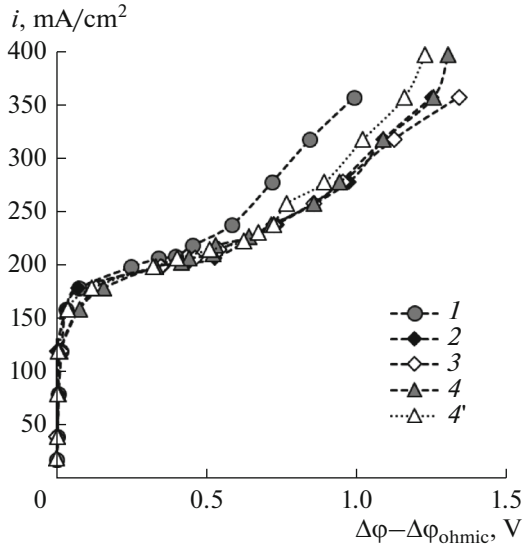

Fig. 5. Current–voltage characteristics of membrane samples: (*1*) MF-4SK, (*2*) MF-4SK-P, (*3*) MF-4SK-R1, and (*4*, *4*) MF-4SK-R2 (surface contacting with (*4*) the cathode and (*4*) the anode in the MEA faces the counterion flux).

and an overlimiting region. The figure shows the reduced current–voltage characteristics excluding the ohmic region.

Note that the most significant effects are observed in the change in the limiting current strength (i_{lim}) and plateau length (Δ), the values of which are listed in Table 3. It can be evident that, for the membranes subjected to thermal and mechanical impacts during pressing, the limiting current plateau length increases by about 50%. A similar effect was observed by a number of authors in studying the effect of the scales of the geometrical heterogeneity of the surface on the parameters of the current–voltage characteristic of an ion-exchange membrane [34].

Analysis of the optical images of the surface of the studied samples shown in Fig. 6 reveals the appearance of geometrical heterogeneities on the membrane surface after pressing; the pattern of the heterogeneities follows the weaving of carbon paper fibers. This factor causes a delay in the onset of the overlimiting state in the electromembrane system. However, it should be noted that the appearance of heterogeneities of this scale does not affect the limiting current strength (Table 3).

For the MF-4SK-R2 sample, an asymmetry of the current–voltage characteristic was found after stress testing; it was not observed for the other samples. In the case where the surface contacting with the cathode in the MEA meets a counterion flux, the limiting current density is lower, and the limiting current plateau is more extended than that in the case of the reverse orientation of the sample. The observed effect of the later transition of the electromembrane system to the overlimiting state can be attributed to the partial degradation of the surface structure due to the appearance of peroxide compounds on the cathode and a decrease in the exchange capacity in the near-surface layer, which, in the case of cluster perfluorinated membranes, leads to an increase in the electrical inhomogeneity of their surface [35].

Table 2. Transport and structural parameters calculated in terms of the microheterogeneous conductivity model

No.	Membrane	f_1	f_2	κ_{iso}, S/m
1	MF-4SK	0.87	0.13	4.08
2	MF-4SK-P	0.86	0.14	2.00
3	MF-4SK-R1	0.88	0.12	2.29
4	MF-4SK-R2	0.87	0.13	1.83

Table 3. Parameters of current–voltage curves

No.	Membrane	i_{lim}, A/m^2	Δ, V
1	MF-4SK	179	0.60
2	MF-4SK-P	174	0.92
3	MF-4SK-R1	170	0.93
4 orientation to the cathode	MF-4SK-R2	164	1.21
4 orientation to the anode		177	0.90

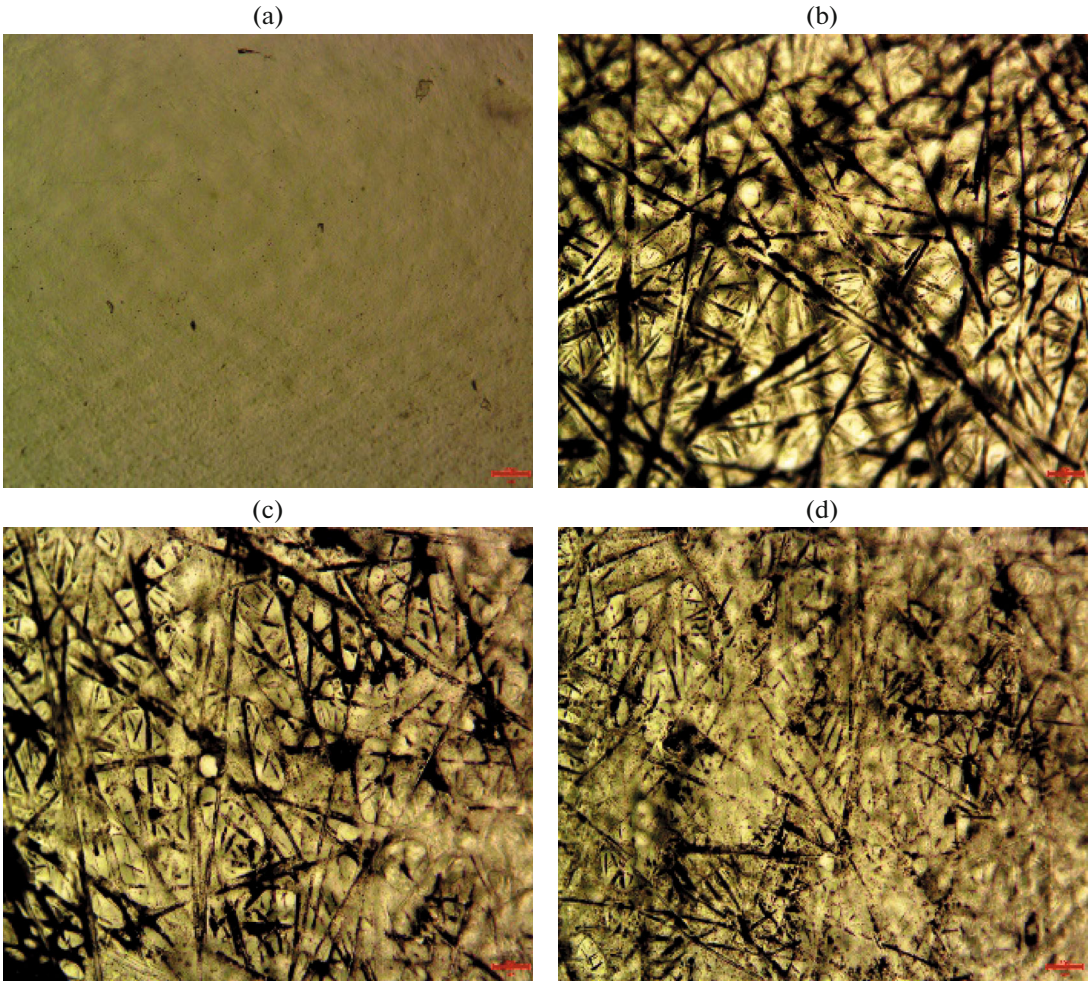

Fig. 6. Optical images of the surface of the studied membranes: (a) MF-4SK, (b) MF-4SK-P, (c) MF-4SK-R1, and (d) MF-4SK-R2.

CONCLUSIONS

A comprehensive study of the transport and structural properties of a polymer electrolyte at different stages of operation of the electrolyte as part of the MEA of a hydrogen fuel cell has been conducted. It has been shown that, after thermal and mechanical impacts on the membrane during the MEA pressing, the membrane thickness, total pore volume, and specific water uptake significantly decrease (by 28%). In this case, the electrical conductivity of the membrane in general and the gel phase decreases twofold; however, the ratio of the volume fractions of the conducting phases remains constant. After operation of the membrane as part of the MEA of a hydrogen fuel cell under mild conditions of the potentiostatic mode, a further deterioration of the physicochemical characteristics of the membranes does not occur. However, the operation of the membrane in the stress testing mode is characterized by an 8% decrease in the exchange capacity and the appearance of an asymmetry of the current–voltage characteristic.

FUNDING

This work was supported by the Russian Foundation for Basic Research (project no. 20-38-90099).

CONFLICT OF INTEREST

The authors declare that they have no conflicts of interest.

REFERENCES

1. P. C. Okonkwo, O. O. Ige, E. M. Barhoumi, P. C. Uzoma, W. Emori, A. Benamor, and A. M. Abdullah, Int. J. Hydrogen Energy **46**, 15850 (2021).
2. A. D. Aliev, L. A. Beketaeva, V. A. Bogdanovskaya, E. V. Burkovskii, et al., Russ. J. Electrochem. **50**, 773 (2014).
3. I. Gatto, A. Carbone, A. Sacca, E. Passalacqua, C. Oldani, L. Merlo, D. Sebastian, A. S. Arico, and V. Baglio, J. Electroanal. Chem. **842**, 59 (2019).
4. I. Pivac, D. Bezmalinovic, and F. Barbir, Int. J. Hydrogen Energy **43**, 13512 (2018).

5. Q. Meyer, Y. Zeng, and C. Zhao, J. Power Sources **437**, 226922 (2019).
6. P. J. Ferreira, G. J. la O', Y. Shao-Horn, D. Morgan, R. Makharia, S. Kocha, and H. A. Gasteiger, J. Electrochem. Soc. **152**, A2256 (2005).
7. Y. Xiao-Zi, L. Hui, Z. Shengsheng, M. Jonathan, and W. Haijiang, J. Power Sources **196**, 9107 (2011).
8. M. V. Martínez-Huerta and M. J. Lázaro, Catal. Today **285**, 3 (2017).
9. A. El-kharouf, A. Chandan, M. Hattenberger, and B. G. Pollet, J. Energy Inst. **85**, 188 (2012).
10. J. Wu, X. Z. Yuan, J. J. Martin, H. Wang, J. Zhang, J. Shen, W. Shaohong, and W. Merida, J. Power Sources **184**, 104 (2008).
11. R. Borup, J. Meyers, B. Pivovar, Y. S. Kim, et al., Chem. Rev. **107**, 3904 (2007).
12. T. Haolin, P. Shen, P. J. San, W. Fang, and P. Mu, J. Power Sources **170**, 85 (2007).
13. A. Sorrentino, K. Sundmacher, and T. Vidakovic-Koch, Energies **13**, 5825 (2020).
14. J. Park, M. A. Uddin, U. Pasaogullari, and L. Bonville, Int. J. Hydrogen Energy **42**, 21146 (2017).
15. M. A. Uddin, J. Qi, X. Wang, U. Pasaogullari, and L. Bonville, Int. J. Hydrogen Energy **40**, 13099 (2015).
16. M. Sulek, J. Adams, S. Kaberline, M. Ricketts, and J. R. Waldecker, J. Power Sources **196**, 8967 (2015).
17. A. Pozio, R. F. Silva, M. D. Francesco, and L. Giorgi, Electrochim. Acta **48**, 1543 (2003).
18. S. A. Grigoriev, D. G. Bessarabov, and V. N. Fateev, Russ. J. Electrochem. **53**, 318 (2017).
19. M. Min and H. Kim, Int. J. Hydrogen Energy **41**, 17557 (2016).
20. A. A. Alekseenko, V. E. Guterman, S. V. Belenov, V. S. Menshikov, N. Yu. Tabachkova, O. I. Safronenko, and E. A. Moguchikh, Int. J. Hydrogen Energy **43**, 3676 (2018).
21. S. Zhang, X. Yuan, H. Wang, W. Mérida, H. Zhu, J. Shen, S. Wu, and J. Zhang, Int. J. Hydrogen Energy **34**, 388 (2009).
22. M. Chandesris, R. Vincent, L. Guetaz, J.-S. Roch, D. Thoby, and M. Quinaud, Int. J. Hydrogen Energy **42**, 8139 (2017).
23. K. Hongsirikarn, X. Mo, J.G. Goodwin, and S. Creager, J. Power Sources **196**, 3060 (2011).
24. K. Teranishi, K. Kawata, S. Tsushima, and S. Hirai, Electrochem. Solid-State Lett. **9**, A475 (2009).
25. S. A. Grigoriev, K. A. Dzhus', D. G. Bessarabov, V. V. Markelov, and V. N. Fateev, Electrokhim. Energ. **14**, 187 (2014).
26. N. P. Berezina, N. A. Kononenko, N. P. Gnusin, and O. A. Dyomina, Adv. Colloid Interface Sci. **139**, 3 (2008).
27. E. D. Belashova, N. A. Melnik, N. D. Pismenskaya, K. A. Shevtsova, A. V. Nebavsky, K. A. Lebedev, and V. V. Nikonenko, Electrochim. Acta **59**, 412 (2012).
28. Y. M. Volfkovich, A. N. Filippov, and V. S. Bagotsky, *Structural Properties of Porous Materials and Powders Used in Different Fields of Science and Technology* (Springer, Verlag London, 2014).
29. Y. M. Volfkovich, V. S. Bagotzky, V. E. Sosenkin, and I. A. Blinov, Colloids Surf. A **187–188**, 349 (2001).
30. N. Kononenko, V. Nikonenko, D. Grande, C. Larchet, L. Dammak, M. Fomenko, and Yu. Volfkovich, Adv. Colloid Interface Sci. **246**, 196 (2017).
31. N. A. Kononenko, M. A. Fomenko, and Yu. M. Volfkovich, Adv. Colloid Interface Sci. **222**, 425 (2015).
32. V. I. Zabolotsky and V. V. Nikonenko, J. Membr. Sci. **79**, 181 (1993).
33. O. A. Demina, I. V. Falina, and N. A. Kononenko, Russ. J. Electrochem. **51**, 561 (2015).
34. J. Balster, M. H. Yildirim, D. F. Stamatialis, R. Ibanez, et al., J. Phys. Chem. B **111**, 2152 (2007).
35. N. D. Pis'menskaya, V. V. Nikonenko, N. A. Mel'nik, G. Pourcelli, and G. Larchet, Russ. J. Electrochem. **48**, 610 (2012).

Translated by M. Timoshinina